NanoBiotechnology

ISSN 1551-1286/05/01:141–152/$30.00
DOI: 10.1385/Nano:1:2:141

Original Article

Optimization of Protein-Based Volumetric Optical Memories and Associative Processors by Using Directed Evolution

Jason R. Hillebrecht,[†,1] Jeremy F. Koscielecki,[†,2] Kevin J. Wise,[1] Duane L. Marcy,[3] William Tetley,[3] Rekha Rangarajan,[1] James Sullivan,[2] Michelle Brideau,[2] Mark P. Krebs,[4] Jeffrey A. Stuart,[3] and Robert R. Birge[,1,2,3]*

[1]Department of Molecular and Cell Biology, University of Connecticut, Storrs, CT 06269, USA; [2]Department of Chemistry, University of Connecticut, Storrs, CT 06269, USA; [3]W. M. Keck Center for Molecular Electronics, Syracuse University, Syracuse NY 13244, USA; and [4]Department of Ophthalmology, College of Medicine, University of Florida, Gainesville, Florida 32610, USA

Abstract

The potential use of proteins in device applications has advanced in large part due to significant advances in the methods and procedures of protein engineering, most notably, directed evolution. Directed evolution has been used to tailor a broad range of enzymatic proteins for pharmaceutical and industrial applications. Thermal stability, chemical stability, and substrate specificity are among the most common phenotypes targeted for optimization. However, in vivo screening systems for photoactive proteins have been slow in development. A high-throughput screening system for the photokinetic optimization of photoactive proteins would promote the development of protein-based field-effect transistors, artificial retinas, spatial light modulators, photovoltaic fuel cells, three-dimensional volumetric memories, and optical holographic processors. This investigation seeks to optimize the photoactive protein bacteriorhodopsin (BR) for volumetric optical and holographic memories. Semi-random mutagenesis and in vitro screening were used to create and analyze nearly 800 mutants spanning the entire length of the *bacterio-opsin* (*bop*) gene. To fully realize the potential of BR in optoelectronic environments, future investigations will utilize global mutagenesis and in vivo screening systems. The architecture for a potential in vivo screening system is explored in this study. We demonstrate the ability to measure the formation and decay of the red-shifted O-state within in vivo colonies of *Halobacterium salinarum*, and discuss the implications of this screening method to directed evolution.

(Nanobiotechnology DOI: 10.1385/Nano:1:2:141)

Key Words: Optical memories; directed evolution; proteins.

***Correspondence and reprint requests to:**
Robert R. Birge
Department of Molecular and Cell Biology, University of Connecticut, Storrs, CT 06269 USA.
[†]These authors contributed equally to this work.

Introduction

The field of nanotechnology has responded to the challenges posed by Moore's law by measuring, modeling, and fabricating materials no larger than one thousandth of a micron (nanometer). At this size, techniques in nanolithography must account for the thermodynamic effects that accompany complex molecular architectures. To cope with the high error rates associated with these thermal side effects, fault-tolerant designs are often used in fabricating such devices. The caveat to using these designs is that they rarely match the high level of functional complexity that is observed in biological machinery. As a result, biological nanotechnology has emerged as an appealing alternative to methods in macroscopic miniaturization *(1)*.

Nearly all forms of life use nano-scale machinery for structural support, motion, metabolism, and information processing. Many of these organic macromolecules have survived multiple extinction events and hostile environmental transformations over the past 3.5 billion years. During this time, genetic mutations have accumulated and manifested into changes in the structure and function of these molecules. If nature can create highly efficient, genetically versatile machines, it is expected that they can be modified to function in biologically based nanoscopic devices. Consequently, directed evolution has become a staple of most endeavors to incorporate organic components into optical and electronic device architectures.

Directed evolution is the process by which proteins are optimized toward a specific characteristic via multiple rounds of genetic mutation and differential selection *(2–7)*. Recent investigations have shown that it is possible to optimize the thermal stability, chemical stability, and substrate specificity of proteins used in therapeutic and industrial applications *(8–12)*. Mutant libraries are first exposed to a selective pressure and then screened for a characteristic of interest. Mutants with favorable phenotypes are genetically characterized and used as parental templates in subsequent rounds of directed evolution. The stringency of each screen is increased in order to drive the mutant library toward a predetermined end point.

While directed evolution has historically been used to optimize organic macromolecules for pharmaceutical and industrial purposes, investigators are now tailoring this technique to optimize photoactive proteins to function in optoelectronic and photovoltaic environments *(12–15)*. This effort has spawned the development of protein-based photovoltaic fuel cells, field-effect transistors, motion-tracking devices, spatial light modulators, artificial retinas, three-dimensional removable memories, and holographic associative processors *(16–25)*.

One of the more unique photoactive proteins to be investigated in the past 20 yr is bacteriorhodopsin (BR). Bacteriorhodopsin is a light-transducing protein that is found within the plasma membrane of the archaea *Halobacteriun salinarum (26,27)*. This transmembrane protein is composed of seven helical segments that are arranged in a two-dimensional hexagonal lattice of trimers *(28)*. This semi-crystalline environment enables the protein to capture light in all polarizations and offers resistance to fluctuations in temperature, radiation, and pH.

The primary light-absorbing moiety in bacteriorhodopsin is an all-*trans* retinal chromophore that is covalently attached to the protein via a protonated Schiff base linkage to Lys-216, shown in Fig. 1A. Upon light absorption, the chromophore isomerizes from all-*trans* to a 13-*cis* configuration. Chromophore isomerization triggers changes in protein structure and protein–chromophore interactions. Changes in the protein–chromophore environment are visualized through a photocycle of spectrally discrete intermediate states labeled bR, K, L, M, N, and O. Figure 1B lists the absorption maximum and lifetime of each spectral intermediate of the BR photocycle. Each photocycle results in the translocation of a proton from the cytoplasmic to extracellular face of the membrane.

When environmental conditions become unfavorable for aerobic respiration, *H. salinarum* expresses BR in what is known as the purple membrane (PM). The proton pumping action of BR leads to the formation of an electrochemical gradient across the cellular membrane. The electrochemical flux triggers membrane-bound ATPase to synthesize ATP for key cellular functions *(29,30)*. The capacity to generate energy via aerobic and photosynthetic pathways has surely added to the evolutionary fitness of *H. salinarum*.

One of the unique features of BR, from the perspective of device applications, is the branched photochemistry of the protein. Upon illuminating the O-state with red light, a branching reaction forms a short-lived P-state that quickly decays to a more permanent Q-state. Both the P- and Q states have a 9-*cis* chromophore that is sterically caged within the apoprotein binding pocket *(31)*. The Q-state is stable for up to 7 yr and is easily recycled back to the bR resting state via illumination with blue light. The optical architectures discussed in this study exploit the branched photochemistry of BR for binary photonic and holographic memory storage devices.

Bacteriorhodopsin-based volumetric memories are designed to read, write, and erase binary data in volumetric cubes of the protein *(24,25)*. Bacteriorhodopsin, in the form of PM fragments, is suspended in a polymer matrix and positioned between a green, red, and blue laser diode. Figure 2 illustrates the process by which data are written, read, and erased from volumetric cubes of BR.

To write data, a single block of the protein matrix is paged with a green laser diode to activate the BR photocycle. Access to the branched photocycle (P- and Q-states) is achieved via illumination with a high-powered red laser diode after approx 2 ms. Because the branched photocycle is only accessed in doubly irradiated pages of the protein matrix, the timing of this binary photonic process is critical to the storage of spatial information.

To read volumetric data, the BR photocycle is once again activated via illumination with a green laser diode. After approx 2 ms, the protein matrix is illuminated with a low-power red laser diode. Low-powered red laser diodes are used so that pages of data stored in the Q-state will transmit the light, whereas pages of data in the O-state will preferentially absorb it. The discrepancy in light absorption is detected as "0" and "1" bits by charge coupled detectors (CCDs) in the memory architecture.

Erasing data stored in the Q-state is achieved by illuminating the data page with a blue laser diode. Illumination with blue light drives the branched photocycle back to the bR resting state. The volumetric memory is designed to accommodate bits stored in either P or Q, and fortunately, both can be erased with blue light. This is not an important issue for a majority of BR variants, but some modifications with enhanced O to P quantum efficiency achieve this increase by decreasing the barrier to all-*trans* → 9-*cis* photochemistry. This genetic

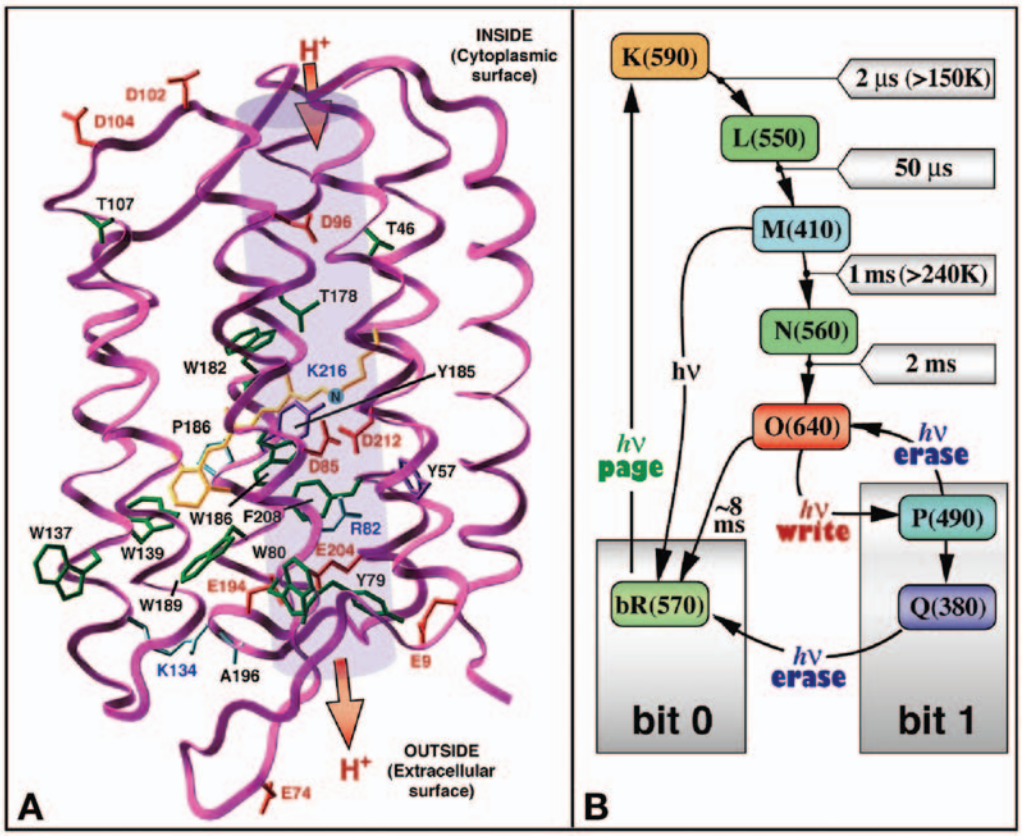

Fig. 1. The structure **(A)** and photocycle **(B)** of bacteriorhodopsin. Amino acids important to the photocycle and proton pumping are shown in panel **(A)**. Panel **(B)** shows the main (bR, K, L, M, N, and O) and branched (P and Q) photocycle intermediates and their associated absorption maxima.

modification invariably decreases the rate of thermal conversion of P to Q, because modifications to the binding site decrease the all-*trans* to 9-*cis* barrier. This yields a binding site that is more compatible to the 9-*cis* protonated Schiff base P geometry. As noted in ref. *24*, the decay of P to Q is driven energetically by repulsive interactions between the 9-*cis* chromophore and the binding site residues (*see* Fig. 6 of ref. *24*).

The branched-photocycle is also of importance to holographic associative memories. Our approach to such memories is based on an adaptation of the Fourier-transform closed-loop holographic memory proposed by Paek and Psaltis *(32)*. Our optical design, shown in Fig. 3, has been discussed previously *(24,33–36)*, and the present discussion will focus primarily on those characteristics of the protein that are critical to function. There are two options available for BR-based holographic memories. If a real-time memory is the goal, then a short-lived intermediate is desired and the M-state is used to store the hologram. If the hologram must be stable for extended periods of time (hours to years), then the M-state is not appropriate and the Q-state is used. Our most recent designs of the associative memory utilize the Q-state, and take advantage of angle tuning to permit multiple Fourier-transform holograms to be stored simultaneously (*see* Fig. 4). Both the M- and Q-states provide excellent diffraction, but the Q-state provides slightly better diffraction efficiency because it has the more blue-shifted absorption spectrum [λ_{max}(Q) = 380 nm, λ_{max}(M) = 410 nm]. The goal of our protein optimization work is to improve the sensitivity of the protein with respect to Q-state formation. Our discussion below examines the use of genetic engineering to achieve this goal.

Semi-random mutagenesis was used in this study to probe the entire length of the *bop* gene for regions that are critical to the formation of 9-*cis* photoproducts. Increasing the yield of the O-state via semi-random mutagenesis represents the first phase of a two-step strategy to optimize the branched photochemistry of the protein. The second phase will introduce global mutations into the region-specific variants selected from the first phase of optimization. Because the structural elements and intramolecular interactions that contribute to the branched photochemistry are ambiguous, global mutagenesis techniques will be used to supplement semi-random optimization.

To efficiently scan the photokinetic properties of thousands of semi-random and random mutants, in vivo screening systems are needed. This study demonstrates that detecting the

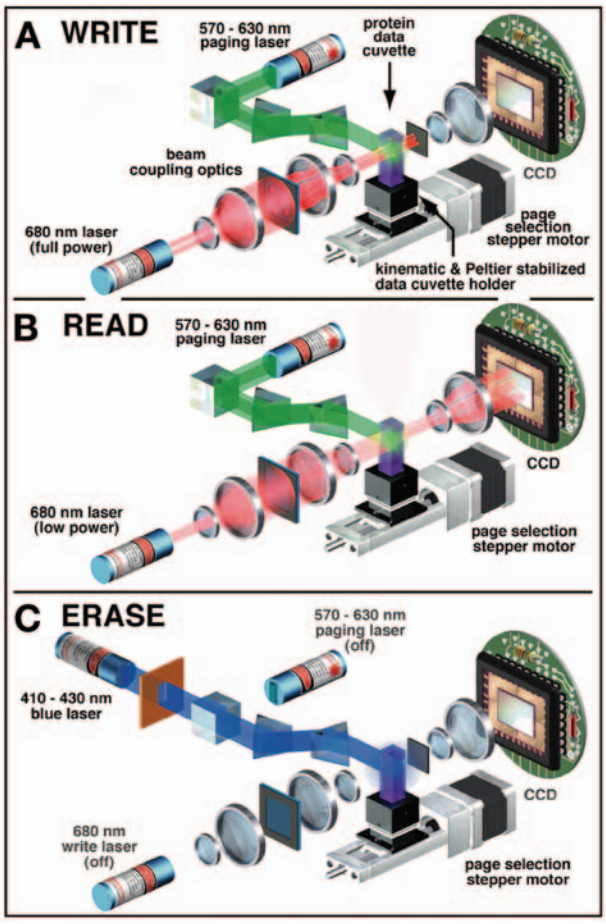

Fig. 2. The write, read, and erase operations of the BR volumetric memory. Both the write and read procedures require two orthogonal laser pulses. The first laser pulse, the "page" beam, activates the BR photocycle in a thin region of the memory. The second laser pulse, the "write" beam, photoconverts a block of the protein from the O-state into the branched photocycle. This "page" and "write" sequence writes a data block into the memory. A similar procedure reads the data block and uses a low-power laser to illuminate the protein. This beam is not absorbed by the data blocks already written in the memory (the O and P intermediates) and the difference of the absorptivity between the written and unwritten data blocks can be detected by an image cast on the CCD. The erase operation uses a third blue laser to erase, or photoconvert, the O and P intermediates back to the BR state. See ref. *24* for a detailed discussion.

formation of 9-*cis* photoproducts in colonies of *H. salinarum* is possible. Future in vivo screening systems will be designed to select for genetically distinct BR variants with high P- and Q-state yields, relative to wild-type protein.

Methods

Semi-random Mutagenesis

Semi-random mutagenesis, also known as saturation mutagenesis, was carried out by the sequence overlap extension (SOE) protocol described in Fig. 5 *(37)*. In short, a three-step polymerase chain reaction (PCR) was used to amplify a 15–20 amino acid region of the *bacterio-opsin* (*bop*) coding sequence. A doped oligonucleotide, with a 20% doping level, was designed to overlap the region of interest. A 20% doping level simply implies that each nucleotide in the "doped region" has a 6.7% chance of being mutated into a different nucleotide. An average of five amino acid substitutions are generated in the doped region of each variant *(13)*. Doped oligonucleotides were synthesized and purchased from the biotechnology center at the University of Wisconsin–Madison.

BR Expression

Following the three-step PCR reaction, the library of semi-random *bop* genes is cloned into the pBA1 expression plasmid *(38)*. The expression system was transformed into *E. coli* according to manufacturer's instructions (Stratagene, La Jolla, CA) and plated onto solid LB media containing ampicillin (50 mg/mL) and incubated overnight at 37°C. Over 2000 genetically distinct colonies were then scraped from the agar plates and pooled together into a single reservoir of cells. DNA was extracted from the mutant library pool using Qiaprep spin prep kit (Qiagen, Valencia, CA) and transformed into *H. salinarum* (MPK409 strain) using standard protocols. The first of the two selection methods in *H. salinarum* use mevinolin to select for true transformants that contain the mevinolin resistance gene encoded within the pBA1 plasmid. Transformants are grown at 40°C on spheroplasting regeneration plates containing mevinolin (4 µg/mL). After 5–7 d of growth, colonies are resuspended in 1 mL of high-salt-culture media, incubated at 40°C for 30 min, and then re-plated onto solid 5-fluoroorotic acid (5-FOA) media. FOA selection guarantees that the ura3::bop locus has been replaced successfully with the functional *bop* gene *(39)*. Without a functional ura3 locus, mutant cells are incapable of synthesizing uracil and will require an outside supplement to survive. Non-recombinants containing the functional ura3 locus will utilize 5-FOA in the pyrimidine biosynthetic pathway and die due to the accumulation of toxic byproducts.

The 5-FOA selection plates are incubated at 40°C for 7–10 d and then placed in a fluorescent light bank for 2–3 d in order to increase the expression of BR. Purple colonies are then picked and replicated in 96-well plates. The first 96-well plate is used to grow the mutant colonies in 200 µL of high-salt media for protein isolation, while the duplicate plate is used to sequence the mutated *bop* genes.

DNA Extraction from H. salinarum

MPK409 genomic DNA was extracted according to the method described in ref. *40*. Briefly, 100 µL of culture at mid-log phase was centrifuged at high speed for 2 min. The pellet was resuspended in 400 µL of milli-Q water; 2–3 µL of the resulting solution were used as a template in the amplification of the *bop* gene using the respective amplification primers. The amplified product was cleaned using a Qiagen PCR purification kit (QIAGEN, Valencia, Calif) and used for direct sequencing.

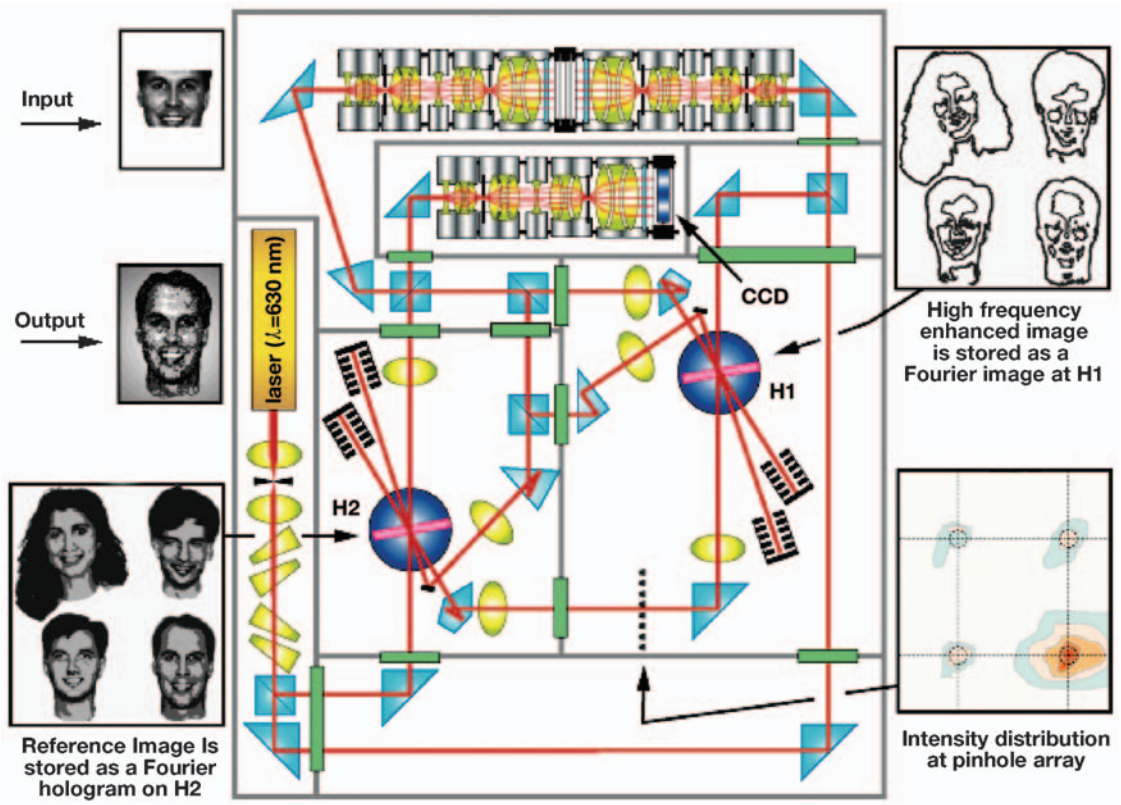

Fig. 3. The Fourier-transform holographic associative memory uses a thin film of BR as a medium for real-time holographic storage. This device can select from thousands of images simultaneously and requires only a partial input image to select and regenerate the entire image from a stored hologram. See ref. *24* for a detailed discussion.

Protein Isolation

MPK409 colonies carrying a wild-type or mutant *bop* gene were inoculated into 96-well plates containing high-salt culture media supplemented with uracil (50 µg/mL). After 1–2 d of active growth at 40°C, 96-well plate cultures were used to inoculate larger volumes (125 mL) of high-salt media enriched with uracil and peptone. *H. salinarum* cultures were actively incubated (200 rpm) at 40°C for 7–10 d under low-oxygen/high-light conditions for enhanced protein expression *(41,42)*.

Protein variants were harvested from *H. salinarum* cultures via low-speed centrifugation (8000 rpm) for 15 min at 4°C. The pellets were re-suspended in 10 mL of milli-Q water containing DNase (0.15 mg/mL) and nutated at ambient temperature for 30–45 min. Purification of PM patches for photokinetic analysis and device testings entailed multiple high-speed spins (50,000 rpm) for 60 min at 4°C using a Beckman Coulter ultra tabletop centrifuge (TLA-55 rotor). The PM pellets were re-suspended in 200 µL of 5-m*M* NaCl.

In Vitro Screening

Type I, an in vitro selection, requires that variant proteins be isolated and purified prior to photokinetic characterization. Genetically distinct proteins were isolated from 250-mL cultures and diluted to an optical density of 1.0 using milli-Q water. UV/Vis measurements were recorded using a Cary 50 spectrometer at ambient temperature. Time-resolved measurements were then performed at 21 ± 1°C, using a 568-nm laser pulse generated by using a Coherent Infinity-XPO Nd:YAG system *(43)*. A rapid scanning monochromater (Olis Instruments, Inc., RSM-1000) was used to collect a fixed wavelength sample spectrum at 412, 568, and 650 nm.

In Vivo Measurement of O-State

The measurement of O-state formation and decay in vivo was accomplished using an intensity stabilized, red laser diode feedback loop to monitor intermediates within a microscopic (2 mm^2) living colony of *H. salinarum*. Scattering is constantly changing during the measurement and the feedback loop adjusts the intensity of the laser to maintain total throughput on both short (<0.1 ms) and long (>1 s) time scales, relative to the median response time of O-state formation. A pulsed green Nd:YAG laser is used to excite the colony and the intensity of the red laser monitored with a 100 ± 50 ms bandpass filter. The formation and decay of the O-state is

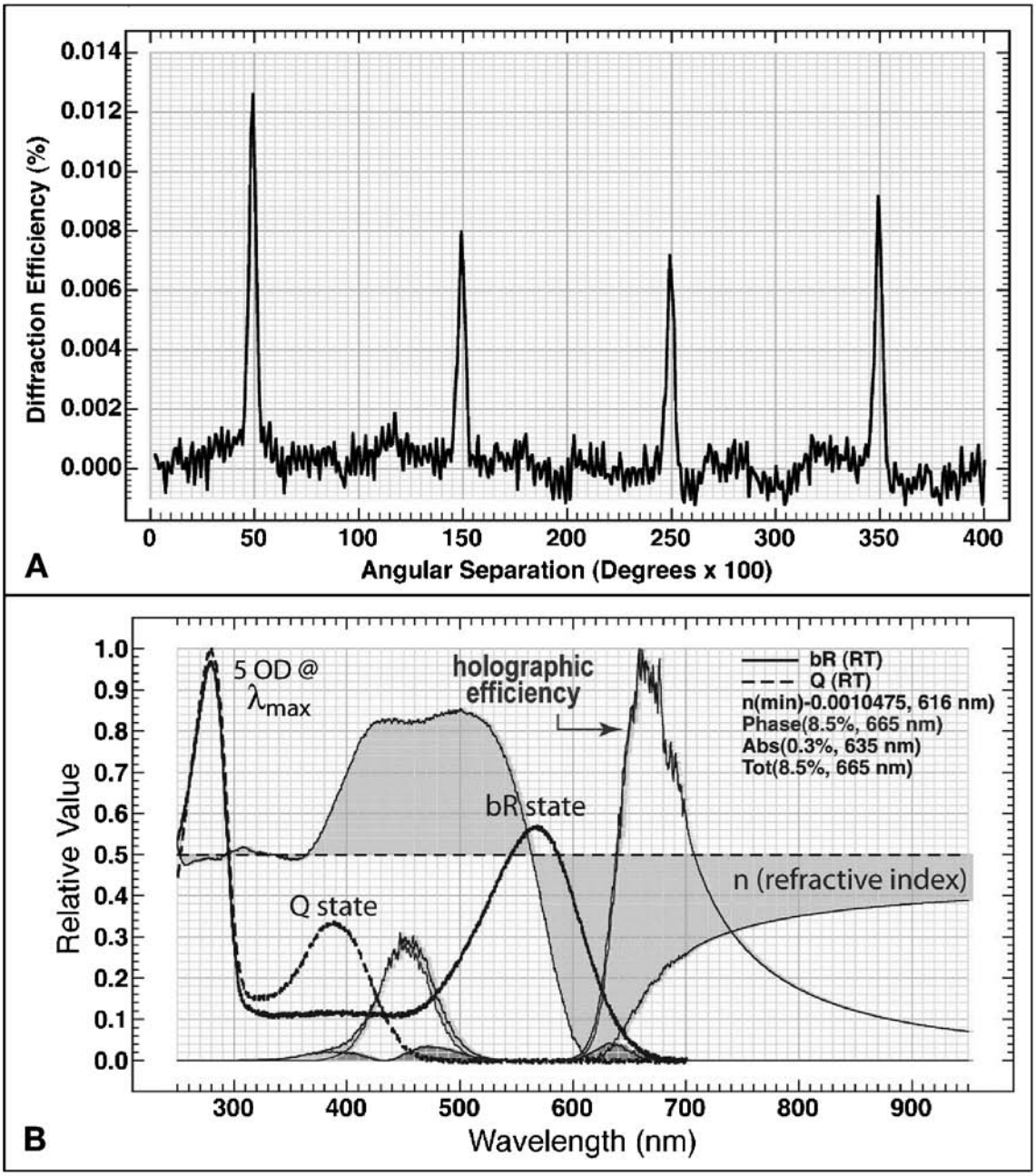

Fig. 4. (A) Q-based diffraction peaks generated from diffraction patterns with one degree angular separation in a 1 cm BR poly(acrylamide) cube with an optical density of 1.5. **(B)** A Kramers–Kronig analysis of wavelength dependence of the diffraction efficiency associated with the formation of the Q-state.

clearly visible although the use of feedback and filtering prevents accurate assignment of kinetic parameters. The peak absorption at 640 nm correlates linearly with the amount of O-state produced.

Results

The first round of semi-random mutagenesis yielded a total of 875 mutants that encompass the entire length of the *bop* gene (1–238). The C-terminus of the protein (239–248) was not included in this study due to restrictions in cloning the gene into the pBA1 expression vector. Figure 6 illustrates the distribution of amino acids in BR that were found to affect the lifetime of the M-state. The majority of BR variants do not have any significant effect on the lifetime of the M-state, relative to the native protein (approx 15 ms). However, a few select mutants were observed to have M-state lifetimes larger than 200 ms. A distribution of BR mutants with significantly longer M-state lifetimes, relative to wild-type protein, is shown in Fig. 7.

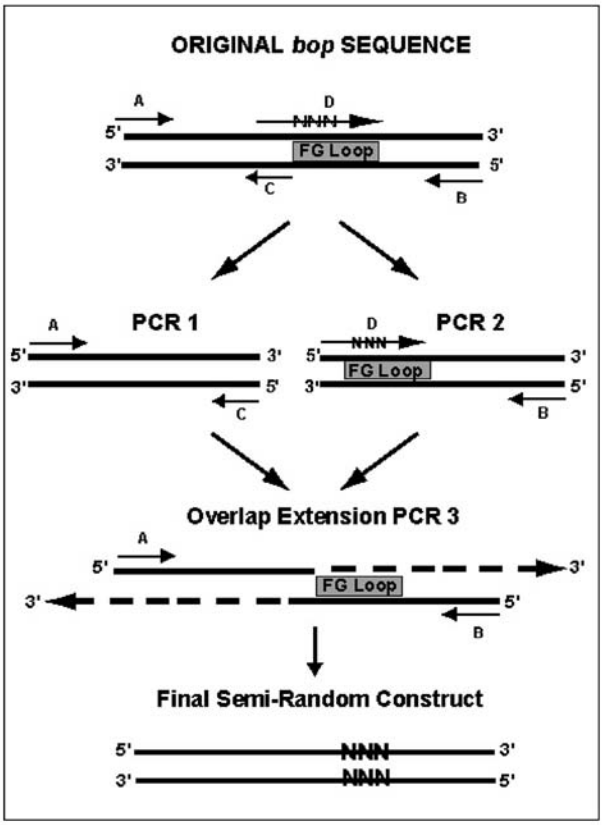

Fig. 5. Semi-random mutagenesis uses a three-step PCR reaction to amplify a specific region of the BR coding sequence. The first step uses four primers (A, B, C, D) to generate two PCR products, one containing a random doped region (in this example the FG loop). The two PCR products are annealed in a subsequent PCR reaction using the A and B flanking primers [adapted from Georgescu et al. *(37)*]. The final construct is then transformed into *H. salinarum* for protein expression and differential selection.

This histogram indicates that BR variants with long M-state lifetimes have one or more mutations in either helix E or F of the protein (139–193).

This study also identified a number of O-state mutants with increased lifetimes. Figure 8 shows that BR variants with long O-state lifetimes, relative to wild type, had mutations that occurred in the FG loop region of the protein. In particular, mutants with O-state lifetimes greater than 50 ms contained mutations located between residues 194 and 208 (Fig. 9). As expected some of these variants contained mutations to Glu194 and Glu204, while others contain a number of other amino acids (up to six mutations in one variant).

Time-resolved UV/Vis spectra of a single colony of *H. salinarum*, shown in Fig. 10, were taken every 5 min at 690 nm for a total of 90 min. Immediately following 2 h of red light illumination (635 nm), additional spectra were taken yielding a lower absorption at 690 nm. The decrease in absorption at 690 nm is indicative of the formation of P and Q. An electronic feedback circuit automatically compensated for the noise created by motion and scattering of the colony, but in the process, modified the temporal response slightly so that the in vivo kinetics could not be accurately assigned. However, the in vivo response data can clearly provide information on the amount of O-state present and changes in the amount of O-state associated with the creation of P and Q.

Discussion

From a device standpoint, optimization of the branched photocycle and key photochemical intermediate states is critical to the efficacy of BR-based binary photonic and holographic memories. Using site-directed mutagenesis to achieve these goals has met with limited success, owing in part to the enormous number of intramolecular associations that contribute to protein functionality. As a result, semi-random mutagenesis has emerged as a valuable tool for elucidating key residues, or a cluster of residues, with unforeseen functional-relevance.

More than 800 semi-random mutants were analyzed for improved M- and O-state lifetimes at 412 and 650 nm, respectively. As expected, the majority of mutants had M- and O-state lifetimes and were comparable to wild-type protein. Previous studies have shown that mutating the aspartic acid at position 96 (the proton-donating group) to asparagine prolongs the lifetime of the M-state to 1050 ms *(44)*. One would expect a long M-state mutant to contain this mutation or one in close proximity to it. Unexpectedly, a triple semi-random mutant (A139G/M145K/L146P) was found to have an M-state lifetime rivaling that of D96N. This mutant does not replace Asp-96, yet has an M-state lifetime of 1100 ms.

Extending the lifetime of the M-state through genetic modification has improved the holographic sensitivity of BR by a factor of 100, relative to the native protein. While optimizing the photokinetics of the M-state is a sound strategy for real-time holographic processing, long-term holographic data storage requires a more permanent photo-intermediate state. Multiple diffraction peaks are observed in Fig. 4, for a two-state holographic system involving the BR resting state and the long-lived Q-state. A single degree of angular separation is observed between each data block. This resolution is characteristic of a high-quality diffraction media in which multiple blocks of data can be stored and read.

To fully realize the potential of Q-based holographic media, the all-*trans* → 9-*cis* barrier must be reduced. Genetic strategies for optimizing the branched photochemistry of BR will potentially include the use of an in vivo screening system designed to select for BR variants with high Q-state yields.

A three-step cell sorting system, shown in Fig. 11, illustrates the scheme by which colonies of *H. salinarum* are screened based on the photokinetic characteristics of the mutated PM. A reservoir of genetically distinct *H. salinarum* cells are mechanically diluted and then screened by sequential optical illumination. Optical selection triggers a high-speed drop selector to either discard the drop or combine it with other desirable mutants. The mutant pool is then subject to three selection steps. The selection strategy includes screening for protein expression,

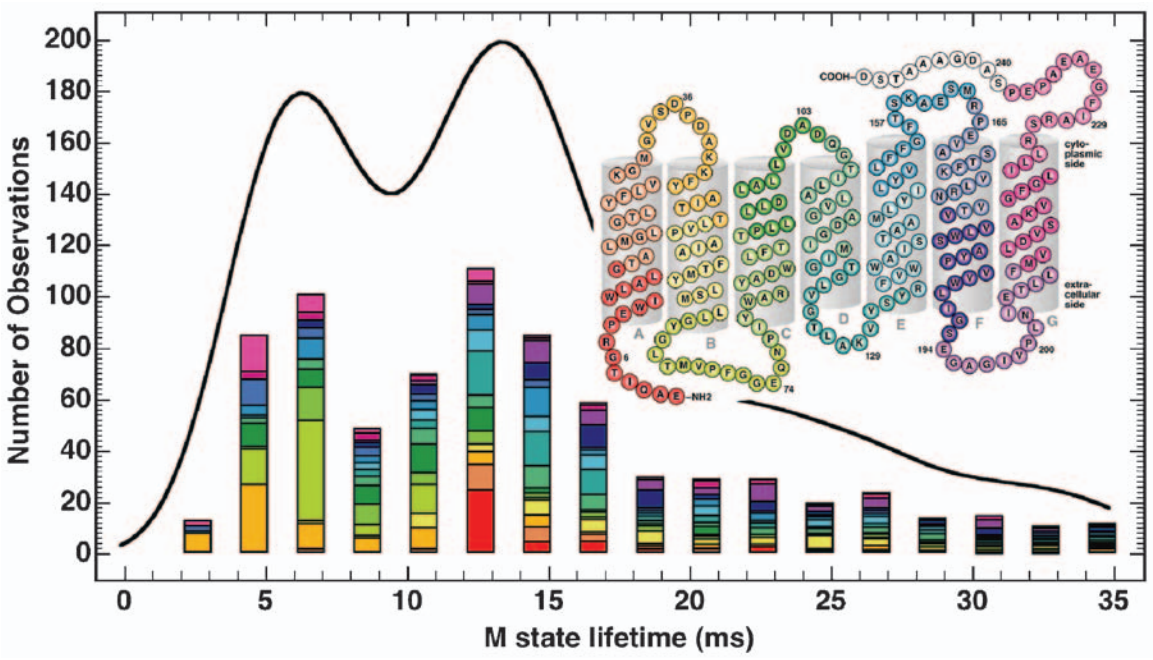

Fig. 6. Histogram showing the correlation between the position of mutated residues and the M-state lifetime. Colors in the bars correspond to similarly colored regions of the secondary structural model of BR (inset).

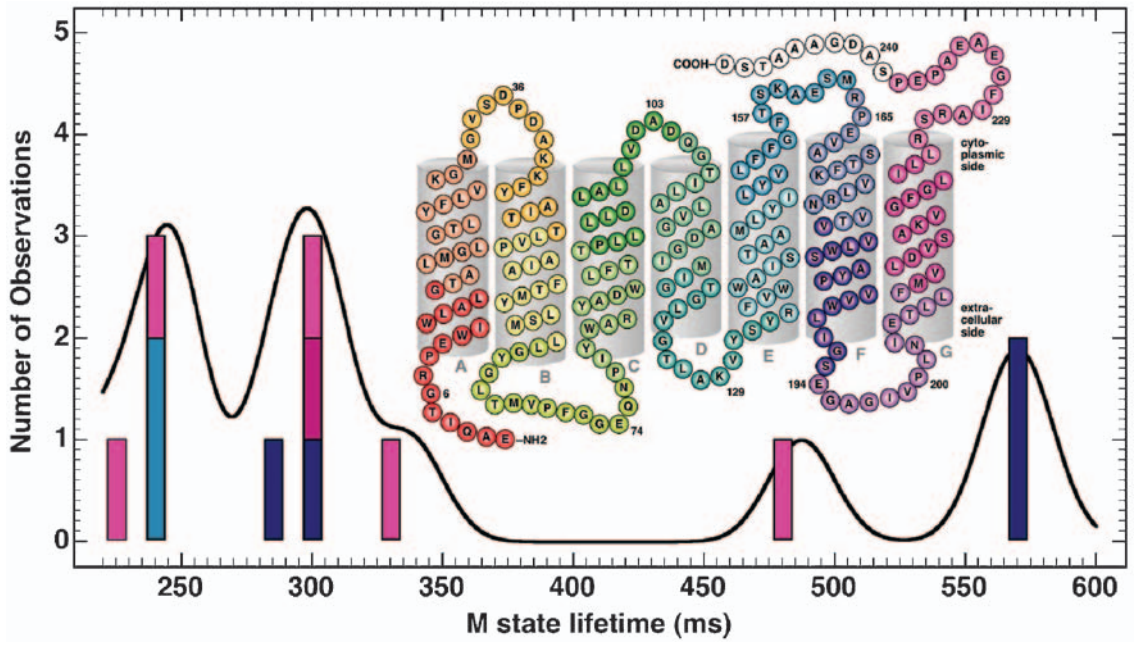

Fig. 7. Histogram analysis of the long-lived M-state lifetimes. The same color scheme is used as in Fig. 6.

branched photochemistry (Q-yield), and organisms containing protein with high quantum efficiencies for the transition from the Q-state back to BR. Organisms that pass the initial screen are inoculated into larger volumes of growth media for sequencing and protein isolation. The holographic efficiency of high Q-yield mutants would then be characterized in an optical recording loop described by Paek and Psaltis.

To genetically tailor BR for binary photonic architectures, a two-step optimization strategy is needed. The primary phase of this endeavor focuses on using semi-random mutagenesis to probe for regions of the *bop* gene that yield attractive O-state kinetics. Improving the lifetime and yield of the O-state can increase the population of P and Q that are formed via binary photonic activation. The second phase of optimization will

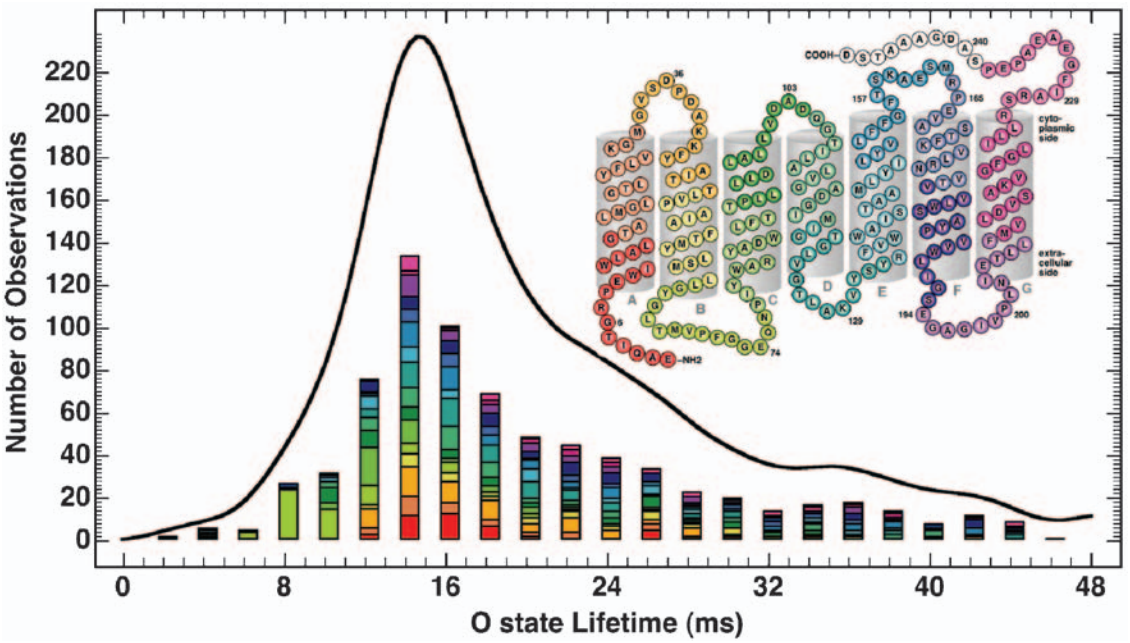

Fig. 8. Histogram analysis of the O-state lifetime of mutants. The same color scheme is used as in Fig. 6.

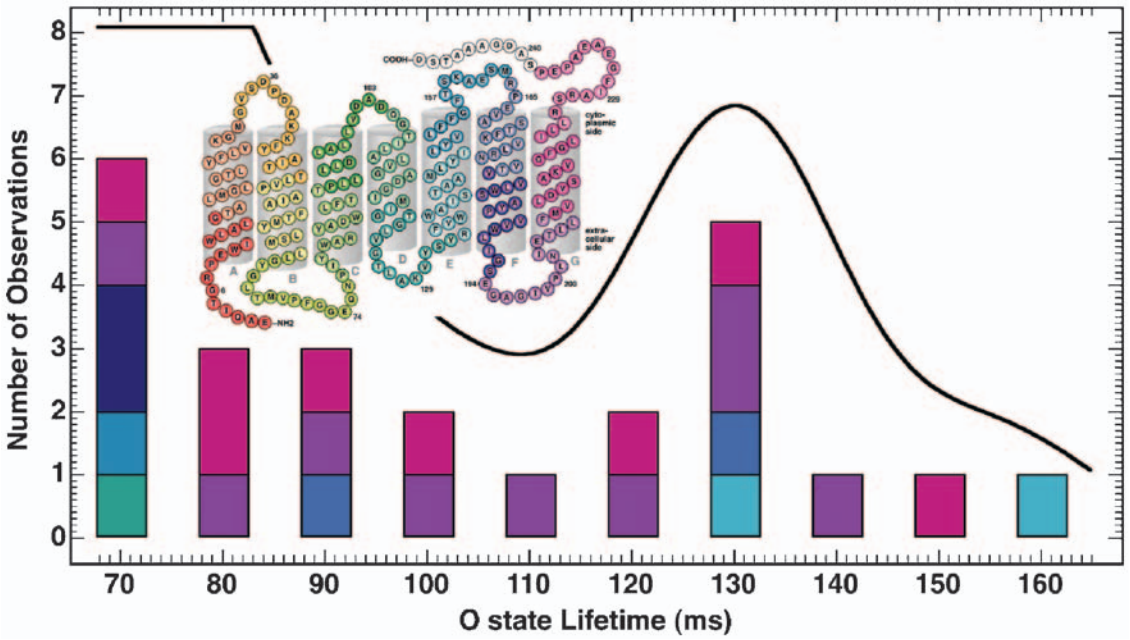

Fig. 9. Histogram analysis of the long-live O-state lifetimes. The same color scheme is used as in Fig. 6.

use select, semi-random variants as templates for global mutagenesis and in vivo screening. These methods will focus on reducing the barrier to the branched photocycle via steric and electrostatic modification of functionally significant residues lining the retinal-binding pocket.

Previous site-directed mutagenesis studies have shown that residues in the FG loop region of the protein are involved with releasing a proton to the extracellular face of the membrane. Two of the most commonly studied residues in the FG loop region are Glu194 and Glu204. Genetic modification of one or both of these residues leads to lengthened O-state lifetimes, relative to the native protein. E194C, E204C, and the double cysteine mutant (E194C/E204C) prolong the lifetime of the O-state by more than 10-fold *(45–47)*.

To increase the scope of site-specific mutagenesis studies, semi-random methods were used to explore the residues

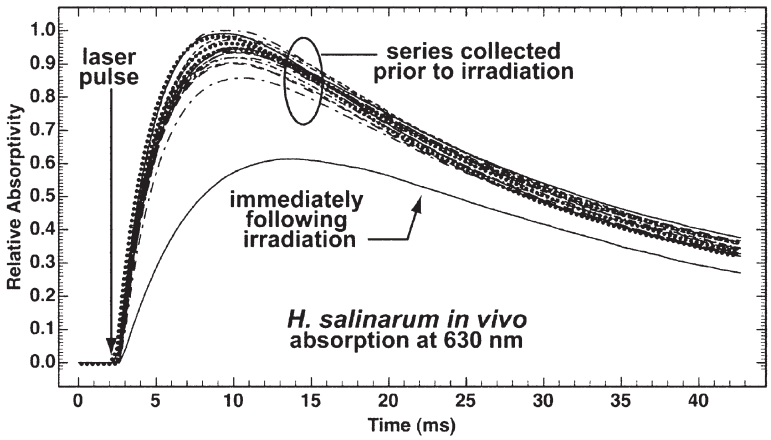

Fig. 10. In vivo photokinetic observation of the O-state within the PM of a microscopic colony of *H. salinarum*. The dashed lines are a measurement of the O-state (690 nm) collected every 5 min prior to 2 h exposure with red light (635 nm). The solid line is measurement of the O-state immediately following the 2 h red light irradiation. The in vivo response data can clearly provide information on the amount of O-state present and changes in the amount of O-state associated with the creation of the Q-state.

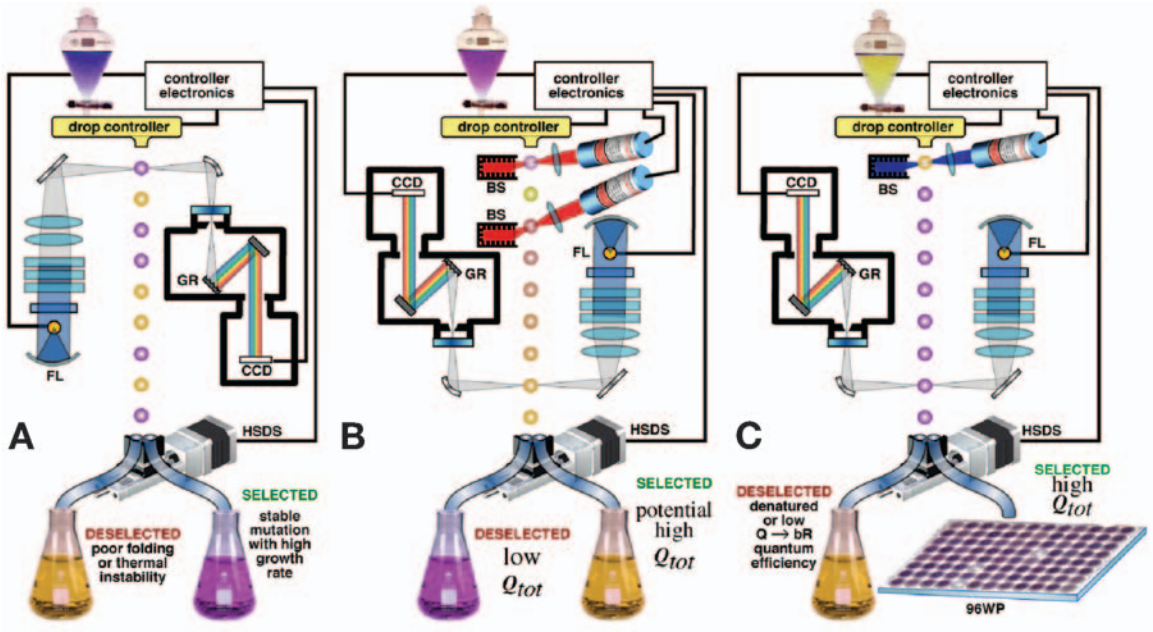

Fig. 11. The three-step cell sorting system allows for in vivo high-throughput photokinetic screening. The first stage **(A)** selects for BR expression and high growth rate. The second stage **(B)** selects mutants with high photochemical conversion into the branched photocycle (O → P transition). The third stage **(C)** selects for mutants having efficient photochemical conversion from the branched photocycle back to the bR state (Q → bR transition). Mutants with desired photochemical characteristics are automatically deposited into a single well of a 96-well plate (96WP).

between position 194 and 206. A sextuple mutant (A196S/I198L/P200T/E204A/T205Q/F208Y) with a 2 s O-state lifetime was generated in the first round of semi-random mutagenesis. The number and type of mutations found in this mutant illustrate the intricacy of the relationships that exist between neighboring amino acids. Future studies will use site-directed methods to determine which residues are actively contributing to the observed photokinetic properties.

To date, the BR mutant with the largest recorded O-state yield is E194Q (Q = 0.327). These data support the contention that Glu194 is a major contributor to the proton translocation pathway. Additional semi-random studies using E194Q as a template for optimization may further enhance the yield of O-state and increase the access to the branched photocycle. It is predicted that up to six rounds of genetic modification may be required before the photochemistry of BR is fully optimized for binary photonic memories.

A high throughput analysis of the *bop* gene will require that techniques in semi-random and random mutagenesis be combined with in vivo screening systems. Figure 9 shows that individual colonies of *H. salinarum* can be indirectly screened for modulations in the branched photocycle of BR at 690 nm. The second phase of the two-step optimization strategy will extrapolate colony-screening technology to whole cell pastes and genetically distinct cultures of *H. salinarum*. The development of in vivo, photokinetic screening systems will broaden the scope of directed evolution to functionally complex photoactive systems.

Conclusions

The lengthened M- and O-state mutants described in this investigation demonstrate that semi-random mutagenesis is key to identifying unforeseen residues, or groups of residues, that shape some identifiable function. While lengthened O-state mutants do not directly relate to optimized branched photochemistry, they are part of a broader strategy to combine region-specific and global mutagenesis techniques. Optimizing the yield of 9-*cis* photoproducts is achievable through in vivo screening techniques described in this study. As in vivo screening technology matures, a broader range of proteins will be genetically tailored to function in optoelectronic environments, as opposed to their native ecosystems.

References

1. Vsevolodov, N. N. (1998), *Biomolecular Electronics. An Introduction via Photosensitive Proteins*. Birkhauser; Boston, 1998.
2. Arnold, F. and Moore, J. C. (1997), *Adv. Biochem. Eng.* **58,** 1–14.
3. Rubingh, D. N. (1997), *Curr. Op. Biotech.* **8,** 417–422.
4. Kuchner, O. and Arnold, F. (1997), *Trends Biotech.* **15,** 523–530.
5. Miyazaki, K. and Arnold, F. H. (1999), *J. Mol. Evol.* **49,** 716–720.
6. Olsen, M., Iverson, B., and Georgiou, G. (2000), *Curr. Op. Biotech.* **11,** 331–337.
7. Arnold, F., Wintrode, P. L., Miyazaki, K., and Gershenson, A. (2001), *Trends Biochem. Sci.* **26,** 100–106.
8. Dalby, P. A. (2003), *Curr. Opin. Struct. Biol.* **13,** 500–505.
9. Kirk, O., Borchert, T. V., and Fuglsang, C. C. (2002), *Curr. Op. Biotech.* **13,** 345–351.
10. Morawski, B., Quan, S., and Arnold, F. (2001), *Biotechnol. Bioeng.* **76,** 99–107.
11. Sterner, R. and Liebl, W. (2001), *Crit. Rev. Biochem. Mol. Bio.* **36,** 39–106.
12. Whaley, S. R., English, D. S., Hu, E. L., Barbara, P. F., and Belcher, A. M. (2000), *Nature* **405,** 665–668.
13. Wise, K. J., Gillespie, N. B., Stuart, J. A., Krebs, M. P., and Birge, R. R. (2002), *T. Biotechnol.* **20,** 387–394.
14. Seeman, N. C. and Belcher, A. M. (2002), *Proc. Natl. Acad. Sci. USA* **99(Suppl 2),** 6451–6455.
15. Hillebrecht, J. R., Wise, K. J., Koscielecki, J. F., and Birge, R. R. (2004), *Methods Enzymol.* **388,** 333–347.
16. Xu, J., Bhattacharya, P., and Varo, G. (2004), *Biosens. Bioelectron.* **19,** 885–892.
17. Li, Q., Stuart, J. A., Birge, R. R., Xu, J., Stickrath, A. B., and Bhattacharya, P. (2004), *Biosens. Bioelectron.* **19,** 869–874.
18. Xu, J., Stickrath, A. B., Bhattacharya, P., et al. (2003), *Biophys. J.* **85,** 1128–1134.
19. Koek, W. D., Bhattacharya, N., Braat, J. J., Chan, V. S., and Westerweel, J. (2004), *Opt. Lett.* **29,** 101–103.
20. Hampp, N. (2000), *Appl. Microbiol. Biotechnol.* **53,** 633–639.
21. Chen, Z. and Birge, R. R. (1993), *Trends Biotech.* **11,** 292–300.
22. Chen, Z., Govender, D., Gross, R., and Birge, R. (1995), *BioSystems* **35,** 145–151.
23. Martin, C. H., Chen, Z. P., and Birge, R. R. (1997), in Proc. Pacific Symp. Biocomputing, R. B. Altman, A. K. Dunker, L. Hunter and T. E. Klein, eds., World Scientific, Maui; pp. 268–279.
24. Birge, R. R., Gillespie, N. B., Izaguirre, E. W., et al. (1999), *J. Phys. Chem. B* **103,** 10,746–10,766.
25. Stuart, J. A., Tallent, J. R., Tan, E. H. L., and Birge, R. R. (1996), *Proc. IEEE Nonvol. Mem. Tech. (INVMTC)* **6,** 45–51.
26. Oesterhelt, D. and Stoeckenius, W. (1971), *Nature (London), New Biol.* **233,** 149–152.
27. Lanyi, J. K. (1999), *Int. Rev. Cytolo.* **187,** 161–202.
28. Sato, H., Takeda, K., Tani, K., et al. (1999), *Acta Cryst. D Biol. Cryst.* **55,** 1251–1256.
29. Birge, R. R. (1981), *Ann. Rev. Biophys. Bioeng.* **10,** 315–354.
30. Ebrey, T. G. (1993), *Light Energy Transduction in Bacteriorhodopsin*, CRC Press, Boca Raton, FL.
31. Popp, A., Wolperdinger, M., Hampp, N., Bräuchle, C., and Oesterhelt, D. (1993), *Biophys. J.* **65,** 1449–1459.
32. Paek, E. G. and Psaltis, D. (1987), *Opt. Eng.* **26,** 428–433.
33. Birge, R. R., Fleitz, P. A., Gross, R. B., et al. (1990), *Proc. IEEE EMBS* **12,** 1788–1789.
34. Gross, R. B., Izgi, K. C., and Birge, R. R. (1992), *Proc. SPIE* **1662,** 186–196.
35. Birge, R. R., Parsons, B., Song, Q. W., and Tallent, J. R. (1997), Protein-Based Three-Dimensional Memories and Associative Processors, Blackweel Science Ltd., Oxford.
36. Birge, B., Fleitz, P., Gross, R., et al. Spatial light modulators and optical associative memories based on bacteriorhodopsin, in Materials Research Society, Boston, MA, 1990.
37. Georgescu, R., Bandara, G., and Sun, L. (2003), *Meth. Mol. Biol.* **231,** 75–83.
38. Krebs, M. P., Hauss, T., Heyn, M. P., RajBhandary, U. L., and Khorana, H. G. (1991), *Proc. Natl. Acad. Sci. USA* **88,** 859–863.
39. Peck, R. F., Dassarma, S., and Krebs, M. P. (2000), *Mol. Microbiol.* **35,** 667–676.
40. Dyall-Smith, M. (2004), *The Halohandbook: Protocols for Halobacterial Genetics*, Melbourne.
41. Oesterhelt, D. and Stoeckenius, W. (1973), *Proc. Natl. Acad. Sci. USA* **70,** 2853–2857.
42. Baliga, N. S., Kennedy, S. P., Ng, W. V., Hood, L., and Dassarma, S. (2001), *Proc. Natl. Acad. Sci. USA.* **98,** 2521–2525.
43. Gillespie, N. B., Wise, K. J., Ren, L., et al. (2002), *J. Phys. Chem. B* **106,** 13,352–13,361.
44. Hampp, N., Popp, A., Bräuchle, C., and Oesterhelt, D. (1992), *J. Phys. Chem.* **96,** 4679–4685.
45. Zscherp, C., Schlesinger, R., and Heberle, J. (2001), *Biochem. and Biophys. Res. Commun.* **283,** 57–63.
46. Balashov, S., Imasheva, E., Ebrey, T., Chen, N., Menick, D., and Crouch, R. (1997), *Biochemistry* **36,** 8671–8676.
47. Brown, L. S., Sasaki, J., Kandori, H., Maeda, A., Needleman, R., and Lanyi, J. K. (1995), *J. Biol. Chem.* **270,** 27,122–27,126.